Applied Thermal Engineering 281 (2025) 128794

Contents lists available at ScienceDirect

Applied Thermal Engineering

journal homepage: www.elsevier.com/locate/ate

Research Paper

Thermo-economic analysis of a geothermal-driven district heating network: Comparison between a water-based and a CO_2-based grid☆

Daniele Fiaschi [a], Pietro Ungar [a,*], Federico Gigliotti [a], Andrés Meana-Fernández [b]

[a] Department of Industrial Engineering, University of Florence, Italy
[b] Thermal machines and Engines Area, Department of Energy, University of Oviedo, Spain

ARTICLE INFO

Keywords:
Geothermal energy
District heating
Thermo-economic analysis
Levelized Cost of Heat (LCOH)
Carbon dioxide

ABSTRACT

The implementation of geothermal-based district heating networks has a substantial impact on mitigating greenhouse gas emissions. Efficient and environmentally friendly heating infrastructures can be established exploiting the heat resources available in existing geothermal reservoirs. Furthermore, the establishment of district heating networks could facilitate a more cost-effective transition towards renewable sources for the end-user, if compared to the need of installing an individual heat pump. This could lead to a reduction in social conflict when pursuing the environmental goals set by policymakers. In this framework, the present work compares two different district heating network layouts: a water-based and a CO_2-based network, with the goal to identify the most promising configuration. While water-based networks are quite known and already installed in multiple locations in Europe, the CO_2-based concept is innovative and could provide significant benefits when coupled with a geothermal reservoir. The network is composed of two pipes, respectively filled with saturated liquid and vapor, at relatively low temperatures (0 °C to 30 °C), and heat is provided to final users by compressing vapor to reach the required outlet temperature. This makes the system very flexible and allows it to operate even with very cold and shallow geothermal reservoirs, thus significantly reducing the installation cost. A complete thermodynamic and economic analysis has been performed for both cases based on an existing geothermal reservoir in Gavorrano (southern Tuscany, Middle Italy), finding that the CO_2 network reduces the necessary drilling depth from 5 to 4 km with respect to water and the Levelized Cost of Heat (LCOH) from 0.21 to 0.16 €/kWh. Although the CO_2-based surface plant can achieve very high COP due to the use of the geothermal well as a heat source, the economic optimum is a COP of 3, since higher COPs would require more heat extraction from the well, increasing drilling costs.

1. Introduction

1.1. General introduction on geothermal energy

As a result of the continuous growth in population and the ongoing process of industrialization, global energy demand increased by 2.2% in 2024 [1] and is expected to continue rising in the coming decades. This increase in energy demand is expected to be met in a sustainable and environmentally responsible manner, transitioning from fossil fuels to more renewable technologies such as wind, solar, biomass, or geothermal energy sources. To decrease carbon emissions, it is also necessary to improve the existing energy systems or develop new technologies that make better energy use. In this context, geothermal energy sources represent a valuable alternative for clean and safe energy generation, with low operating costs compared to other systems [2]. In addition, they are not subject to weather variability, thereby providing a stable and continuous supply of energy in contrast to wind and solar energy.

Despite its vast potential and its theoretical availability everywhere on the Earth's surface, the economic viability of geothermal electricity generation has been demonstrated only in limited regions characterized by a very high geothermal gradient. In 2023, more than 90% of global geothermal electricity generation was concentrated in 10 countries [3]. On the other hand, the direct use of geothermal energy for heating/cooling applications, requiring a lower fluid temperature, is prone to be used in less promising geothermal areas too. Consequently, about 75% of geothermal energy generation is used for district heating applications [4], where low and medium-temperature sources can be exploited [5].

☆ This article is part of a Special issue entitled: 'SDEWES 2024' published in Applied Thermal Engineering.

* Corresponding author.
E-mail address: pietro.ungar@unifi.it (P. Ungar).

https://doi.org/10.1016/j.applthermaleng.2025.128794
Received 27 January 2025; Received in revised form 17 September 2025; Accepted 19 October 2025
Available online 22 October 2025
1359-4311/

Nomenclature

Acronyms

CLGS	Closed Loop Geothermal System
COP	Coefficient Of Performance
DHN	District Heating Network
HDD	Heating Degree Days, ° C
LCOH	Levelized Cost Of Heat, c€/kWh

Economics

C_f	System Capacity Factor
$C_{\square}$	Absolute cost, €
$c_{\square}$	Specific cost, €/kWh
c_{el}	Electricity cost, €/kWh
h_y	Hours in one year, *hours/year*
i	Interest rate
L_e	System operational life, *years*
OM_{ratio}	Yearly Operation and Maintenance Ratio

Geometrics

$\phi_{\square}$	Pipe Diameter, m
$A_{\square}$	Area (Heat Exchanger), m^2
$depth$	Well Horiz. Section Depth, m
$length$	Well Horiz. Section Length, m
n_{wells}	# of well to be drilled

Other

A_p	Population density, m^2*/person*
EP_{li}	Energy Performance Index
Pop	Population of a municipality
S_f	Building Shape Factor

Geology

α_{rocks}	Rocks Thermal Diffusivity, m^2/s
$grad$	Geothermal Gradient, °C/m
k_{rocks}	Rocks conductivity, W/m K
T_{rocks}	Undisturbed Rock Temperature *(at depth)*, ° C
T_{surf}	Undisturbed Rock Temperature *(surface)*, ° C

Subscripts

DH	District Heating
he, i	ith heat exchanger of the DHN
i	ith branch of the DHN
in	input *(in the surface plant)*
out	output *(from the surface plant)*

Thermodynamics

$\Delta h_{\%}$	Well Spec. Heat Increase Fraction
Δh_{max}	Maximum Well Spec. Heat Increase
$\dot{m}_{\square}$	mass flow, kg/s
$\dot{Q}_{\square}$	Thermal power, kW_t
$\dot{q}_{\square}$	Spec. Thermal power, kJ_t/kg
$\dot{W}_{\square}$	Mechanical/Electrical power, kW_e
DT_{HE}	Heat Exchanger Pinch Point, ° C
HE_{eff}	Effectiveness of the regenerator (CO_2-*based*)
p_{perc}	Adimensionalized maximum pressure (CO_2-*based*)
R_{rocks}	Rocks Thermal Resistance, m^2K/W
$T_{\square}$	Temperature, ° C
T_{perc}	Adimensionalized maximum temperature *(water-based)*
T_{supply}	Fluid Temperature in the DHN (CO_2-*based*), ° C
$v_{\square}$	Fluid Speed in pipeline, m/s

1.2. Geothermal powered district heating networks

With a significant part of global energy consumption being related to energy use in buildings, District Heating Networks (DHNs) will likely become vital in modern urban energy systems, as they can supply heat to residential, commercial, and industrial sectors in an efficient manner [6]. Over the recent decades, they have attracted significant attention in the scientific community as a valuable strategy to control greenhouse gas emissions [7], improve energy security, and help to reduce the cost of the required energy transition from fossil fuels [8] if compared to the need of installing individual user heat pumps. All these factors could lead to a reduction in social conflict when pursuing the environmental goals set by policymakers.

One of the advantages of district networks is their adaptability to different heat sources, ranging from industrial waste heat to the integration of renewable energy sources and the use of high-efficiency heat pumps [9,10]. In this context, the integration of accessible geothermal heat renewable resources into DHNs is highly appealing due to their economic viability. Considering the versatility of geothermal energy as a heat source, coupling geothermal sources into district heating networks is an already proven concept to supply heating energy to whole neighborhoods located near regions with geothermal activity [11]. Many geothermal-based networks are being developed throughout Europe, especially in regions with high capacity factors, such as northern countries [12], which make facilities highly profitable. The range of prices (Levelized Cost of Heat, LCOH) varies depending on the specific locations, but has kept below 0.14 €/kWh in the recent literature [13–16].

Although water has traditionally been the heat transfer fluid for both geothermal wells and DHNs in almost all developed projects, its substitution with alternative fluids has been receiving increasing support from the scientific community. This substitution is particularly interesting when dealing with Closed-Loop Geothermal Systems (CLGS), where a direct contact between the fluid and the rocks is avoided. Among these new-generation working fluids, carbon dioxide has emerged as one of the most promising candidates. This is mainly due to the interesting properties of CO_2, such as its considerably lower viscosity than water, resulting in potentially reduced piping pressure losses [17]. In addition, CO_2 systems can use the latent heat of vaporization at low temperatures, whereas water systems only rely on sensible heat. In the specific context of mid-low temperature geothermal reservoirs, CO_2 changes its density drastically when heated up, generating a thermosiphon effect which may be used to increase fluid flow rate and power extraction [17–19]. Furthermore, this effect can generate a pressurization of the fluid at the well head, which can be beneficial for electricity generation [19–22].

Following the proposal of CO_2-based DHNs by Weber and Favrat [23], the concept has been analyzed and extended by other researchers, showing a high potential for similar applications [24]. Nevertheless, despite the potential of this technology, the share of geothermal sources in district heating and cooling is still considerably low [25], emphasizing the necessity of performing more numerical and experimental studies for these innovative designs.

Table 1
Interpolation parameters for EP_{li}.

	a	b	c	d
1	$6.28{\cdot}10^{-9}$	$-3.68{\cdot}10^{-5}$	$8.73{\cdot}10^{-2}$	$-1.80{\cdot}10^{0}$
2	$-2.87{\cdot}10^{-9}$	$1.5{\cdot}10^{-5}$	$-1.24{\cdot}10^{-2}$	$3.30{\cdot}10^{0}$

1.3. Research gap and scope of this work

Numerous studies in the literature propose innovative designs integrating multiple interconnected components and systems, with the objective of producing various outputs while enhancing both energy and exergy efficiencies. However, these studies often lack empirical operational data or comprehensive techno-economic assessments. Furthermore, the majority of such works concentrate on optimizing either the sub-surface or the surface plant in isolation, without conducting an in-depth analysis of their interconnection. This limitation is particularly evident in the context of district heating network applications, where the modeling of one of the sub-systems is frequently oversimplified. The present study uses real data from a geothermal reservoir in Gavorrano (south Tuscany, Italy), a case study [26] part of the HOCLOOP European project [27]. The objective of the study is to compare two alternative working fluids for a potential district heating network, namely carbon dioxide and water. Carbon dioxide has been suggested to perform better in the literature, but the economic aspects have to be considered. The choice of fluid affects the network layout and working temperature, resulting in different drilling depths and system efficiencies. In this sense, this work presents an innovative closed-loop geothermal district heating network, providing a reliable comparison between two alternative configurations based on a thermodynamic and economic analysis. The results contribute to highlight the potential of carbon dioxide as a DHN fluid carrier, especially in the context of using geothermal energy as a thermal energy source.

2. Methodology

This work analyzes the performance of a potential heating network located in Gavorrano, Italy, leveraging its significant geothermal resources [28]. The use of CO_2 or water as working fluids has been studied to select the most appropriate alternative. The following sections present the procedure adopted for the estimation of the network power demand from available real data, the development of models for the water- and CO_2-based heating networks with their corresponding well geometry design, and the economic analysis.

2.1. Estimation of the network power demand

The heating demand in the area was estimated considering the limit energy performance index of the buildings (EP_{li}, as defined by Italian legislation [29]). This value represents the maximum allowable annual energy consumption per square meter of residential buildings as a function of the heating degree-days (HDD) and the building shape factor (S_f). Italian legislation provides a table with different values for EP_{li} for a set of HDD and S_f. A continuous curve was generated by interpolating these discrete values using the following equation:

$$EP_{li} = (a_1 S_f + a_2) \cdot HDD^3 + (b_1 S_f + b_2) \cdot HDD^2 + \cdots + (d_1 S_f + d_2) \quad (1)$$

with the equation parameters collected in Table 1.

With this relationship between EP_{li}, HDD and S_f, the annual energy demand of the network was estimated from the area population using the following equation:

$$Q_{tot} = 1.5 \cdot EP_{li}(HDD, S_f) \cdot Pop \cdot A_P \quad (2)$$

where Pop and A_P are the population and the useful area required in m^2 per person. The values of S_f and A_P have been set to 0.6 and 33 m^2/person, according to standard Italian values. A 1.5 safety factor has been considered, as, unfortunately, many Italian buildings still do not comply with the legislation because they were built before the law came into force in 2010.

2.2. District heating network model

The scheme of the proposed heating networks is shown in Fig. 1.

The main heating network is coupled to the geothermal boreholes and feeds several sub-networks for each municipality. The sub-networks have been designed as medium-temperature networks, with 80 °C supply temperature and 40 °C return temperature [30].

The water-based layout proposed is illustrated in Fig. 1a. The mass flow rate required by each substation ($\dot{m}_{he,i}$) was determined by performing energy balances across the N corresponding heat exchangers:

$$\dot{m}_{he,i} = \frac{\dot{Q}_i}{c_p\left(T_{w,in} - T_{w,out}\right)} \quad (3)$$

Once the individual contributions were established, the total mass flow rate circulating within the network ($\dot{m}_0$) and through the well was computed as:

$$\dot{m}_0 = \sum_{i=1}^{N} \dot{m}_{he,i} \quad (4)$$

The mass flow rate in each branch of the supply line was then derived by applying the principle of mass conservation at each *i-th* node:

$$\dot{m}_i = \dot{m}_{i-1} - \dot{m}_{he,i} \quad (5)$$

The flow rates in the return line were evaluated similarly, with the difference that the mass flow rates associated with the respective heat exchangers were incrementally added at each downstream node. Once the mass flow rates were determined, pipe diameters were calculated by imposing an upper limit on the fluid velocity within the pipes, denoted as v_{max}. The corresponding diameters were then obtained using the following expression:

$$\phi_i = \sqrt{\frac{4\dot{m}_i}{\pi \rho v_{max}}} \quad (6)$$

Finally, pressure losses along the main network pipes were calculated using the Churchill correlation [31].

A similar methodology was applied to the CO_2-based layout, illustrated in Fig. 1b. However, several modifications were necessary to account for the higher complexity of the system. In particular, the working fluid was treated differently in the supply and return lines. It was assumed that carbon dioxide is supplied as saturated vapor and returns as saturated liquid, providing heating power through its latent heat of vaporization. Given its relatively low critical temperature ($T_{crit} \simeq 31$ °C), reaching the operating temperature at the substation heat exchangers requires compressing the vapor through a regenerative cycle. Consequently, the mass flow rate required by each substation ($\dot{m}_{he,i}$) depends on the thermodynamic optimization of the heat pump unit, which involves parameters such as compressor outlet pressure and bypass ratio. An additional difference lies in the fact that the total mass flow rate that circulates within the network ($\dot{m}_0$) is not the same as the well mass flow rate, due to the introduction of a separator. As a result, the flow rate at the well was calculated by performing mass and energy balances within the separator. Finally, at the well outlet, a turbine was incorporated to recover energy from the natural pressurization generated by the CO_2 thermosiphon effect.

The parameters of the network are collected in Table 2. CO_2 saturation temperature in the main network (called, T_{supply}) was varied between 10 and 25 °C to identify the optimal one.

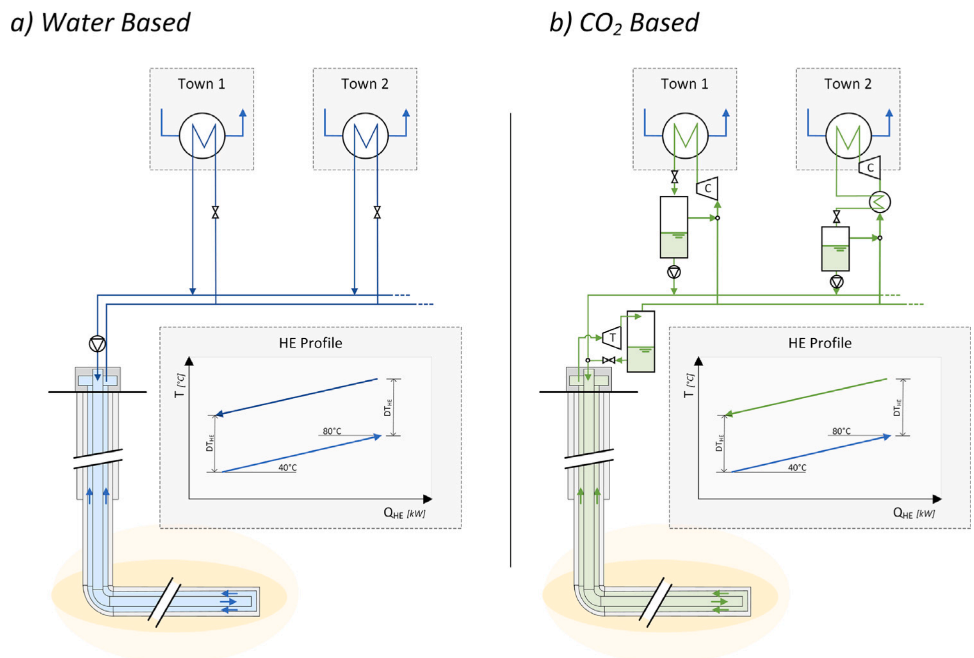

Fig. 1. Scheme of the proposed heating networks: (a) water-based, (b) CO_2-based.

Table 2
System model parameters.

Parameter	Value	Description
DT_{HE}	5 °C	Temperature difference at main heat exchanger
$v_{max,w}$	2 m/s	Maximum water speed inside pipes
$v_{max,CO_2,l}$	1 m/s	Maximum liquid CO_2 speed inside pipes
$v_{max,CO_2,v}$	1.5 m/s	Maximum vapor CO_2 speed inside pipes
η_{pump}	85%	Pump isentropic efficiency
η_{comp}	75%	Compressor isentropic efficiency

2.3. Well model

2.3.1. Simplified well model

As described in [32] and illustrated in Fig. 2, the simplified well model was divided into three sections: the *descending section* (0-1), the *heat exchange section* (1-2), and the *ascending section*. This reflects the geometry of the proposed well in the HOCLOOP solution, consisting of a vertical section to reach the target rock depth and a horizontal section to increase the heat transfer surface area between rock and fluid, as shown in Fig. 1.

The *ascending* and *descending sections* were modeled under the adiabatic assumption, with pressure losses neglected. As already detailed by Di Pippo [33], the governing equations under these hypotheses are:

$$\Delta h = \pm g\ depth \tag{7}$$

$$\Delta s = 0 \tag{8}$$

The sign of the enthalpy change depends on the fluid direction (+ for descending fluid, - otherwise).

The *heat exchange section* was also be modeled in a simplified manner: outlet conditions were evaluated by neglecting pressure losses and assuming that the fluid retrieves only a fraction ($\Delta h_{\%}$) of the maximum heat that can be exchanged (Δh_{max}):

$$h[2] = h[1] + \Delta h_{\%}\ \Delta h_{max} \tag{9}$$

$$p[2] = p[1] \tag{10}$$

The maximum heat that can be exchanged in the heat exchange section was evaluated under the condition at which the fluid reaches the temperature of the surrounding rocks at the section outlet:

$$\Delta h_{max} = h(T = T_{rocks};\ p = p[1])\ -\ h[1] \tag{11}$$

$$T_{rocks} = T_{surf} + depth\ grad \tag{12}$$

$\Delta h_{\%}$ is a design parameter related to the overall length of the well. For this reason, it represents one of the most important parameters to be optimized.

The relation between the well length and $\Delta h_{\%}$ is the following (see Appendix for a full derivation):

$$length = R_{rocks} \frac{\dot{m}\Delta h_{max}}{\pi \phi_{well}} \int_0^{\Delta h_{\%}} \frac{dh'}{\Delta T(h')} \tag{13}$$

Where $\Delta T(h)$ is the temperature difference between undisturbed rocks and the working fluid at a given enthalpy level h. As the fluid is heated up by the surrounding rocks, its temperature and enthalpy increase, and $\Delta T(h)$ is reduced, requiring a higher heat exchange surface for the following pocket of heat.

R_{rocks} is the thermal resistance of the rocks whose definition reflects the degradation of the thermal conductivity over time due to the cooling of the layer of rocks closer to the well, whose effect can be seen in Fig. 4. This is done using a correlation developed by Ungar [32], based on the work of Zhang et al. [34] (again see Appendix for the R_{rocks} correlation).

This relationship allows to determine $length$ once the integral on the left-hand side of Eq. (13) is numerically computed, as shown in Fig. 3. That integral needs to be reevaluated only if inlet fluid conditions or geological parameters ($grad$ or $depth$) change. This makes the code highly efficient for exploring the impact of varying well lengths.

As a final remark, it should be noted that, due to the formulation of the correlation used to evaluate R_{rocks}, our model sizes the well to ensure the required power production even after 20 years of continuous operation. Consequently, the well is oversized with respect to actual needs, since the real extracted power will be lower, which results in a slightly higher final LCOH. This overestimation is expected to remain limited, as the performance degradation of well with diameters around 20 cm usually stabilizes after the first year (see Fig. 4). Nonetheless, the use of this correlation is justified by its simplicity, which enables very fast calculations and facilitates an extensive exploration of the design space.

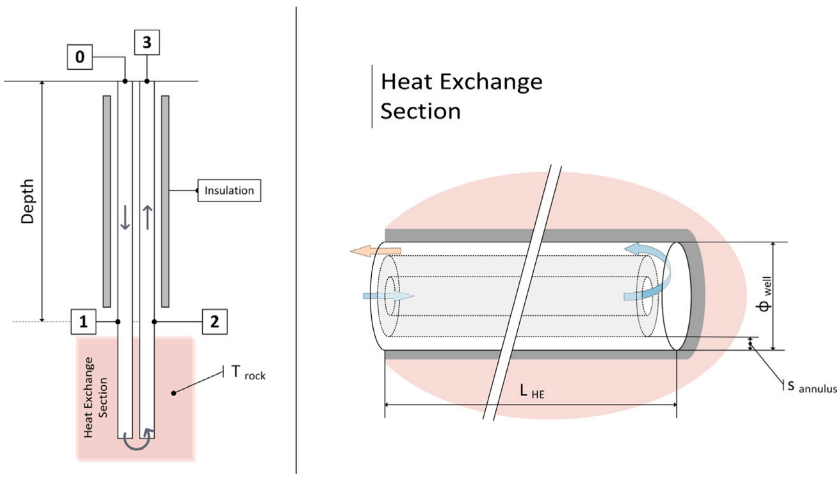

Fig. 2. Scheme of a BHE well as the one analyzed in the HOCLOOP project.

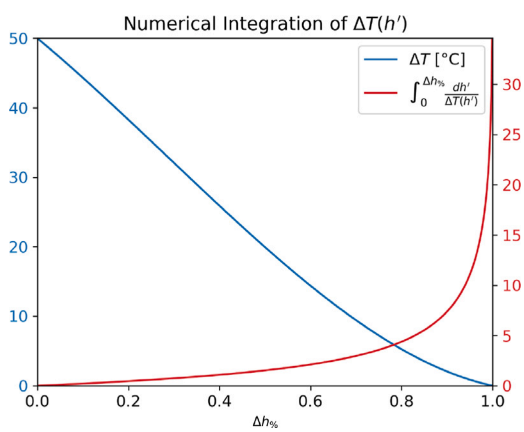

Fig. 3. Example of the numerical evaluation of $\int_0^{\Delta h_{\%}} \frac{dh'}{\Delta T(h')}$. Larger values of $\Delta h_{\%}$ yield higher integral values and, from Eq. (13), lead to longer wells.

2.3.2. Model validation

The proposed model has been validated against the results published by Wanger et al. [35]. The comparison is shown in Fig. 4.

The agreement between the models is remarkable, especially considering that the model proposed in this work is intentionally simplified to enable overall coupled optimization, whereas the model developed by Wanger et al. is a detailed representation of the well, accounting for heat transfer in the descending section as well as between the annulus and the tubing.

The differences observed can be attributed to these assumptions: at shallower depths, the increase in heat transfer due to the heat exchange in the vertical section is negligible, leading the simplified model to overestimate performance since it neglects internal heat transfer. Conversely, at greater depths, vertical heat transfer becomes more significant, causing the simplified model to underestimate well performance. For wells of about 3 km depth (in this particular case study), these two effects counterbalance each other.

2.4. Economic analysis

The LCOH was evaluated following the same approach used by Ungar et al. [36]:

$$LCOH = \frac{C_{tot}\beta + \dot{W}_{tot}c_{el}}{\dot{Q}_{DH}}, \quad \beta = \frac{1+\alpha OM_{ratio}}{\alpha C_f h_y}, \quad \alpha = \frac{1-(1+i)^{-L_e}}{i} \tag{14}$$

where C_{tot} is the total investment cost predicted for the installation of the network, $\dot{W}_{tot}$ and $\dot{Q}_{DH}$ are the design electrical power and heating demands, OM_{ratio} is the annual rate of operation and maintenance cost with respect to the initial investment (assumed to be 5%), and L_e and i are the life expectancy of the DHN (20 years) and the annual interest rate (4%) respectively. c_{el} = 12c€/kWh is the average electricity price in Italy in Sept. 2024 [37]. Finally, h_y = 8760 h/year is the number of hours in a year, while C_f = 33% is the capacity factor estimated in Section 3.2. The total investment cost C_{tot} was evaluated with the correlations reported in Table 3.

3. Gavorrano case study

3.1. Description of the geothermal resource

For the purposes of this study, a closed-loop configuration is considered, wherein there is no direct contact between the working fluid and the geothermal fluid. As a result, the most critical parameter influencing the analysis is the average geothermal gradient. Based on the findings of Garzonio et al. [44], this gradient was estimated to be approximately 75 °C/km. This value is consistent with the data reported by Baldi et al. [45] for southern Tuscany, where the geothermal gradient in peripheral areas of the field does not fall below 70 °C/km. Due to this condition, the Gavorrano geothermal area was considered suitable for testing the potential of CO_2 closed loops for a local district heating application. Fig. 5 shows the area selected for the case study, where the different municipalities and key industrial areas are highlighted. The geothermal resource, located near Gavorrano, is highlighted in light green at the bottom-right corner of the map, and the proposed district heating network is depicted in orange.

3.2. Estimation of the power demand for each municipality

The methodology outlined in Section 2.1 was employed to estimate the power demand for the municipalities included in the analysis: Gavorrano, Bagni di Gavorrano, Scarlino Scalo and Follonica, as illustrated in Fig. 5. To have a better estimate of the behavior of the network throughout the year, data from an existing DHN in Calenzano [24], a small town near Florence, have been used and scaled to identify the maximum power demand throughout the year ($\dot{Q}_{max}$) and the expected capacity factor (C_f). The power demand measured in the Calenzano network throughout a year, shown in Fig. 6, was scaled to match the predicted demand for each municipality in the Gavorrano area.

For the purposes of this work, only the winter months (the unshaded part of Fig. 6, from the beginning of October to the end of April) were considered. The reason is that the DHN in Calenzano is used to power

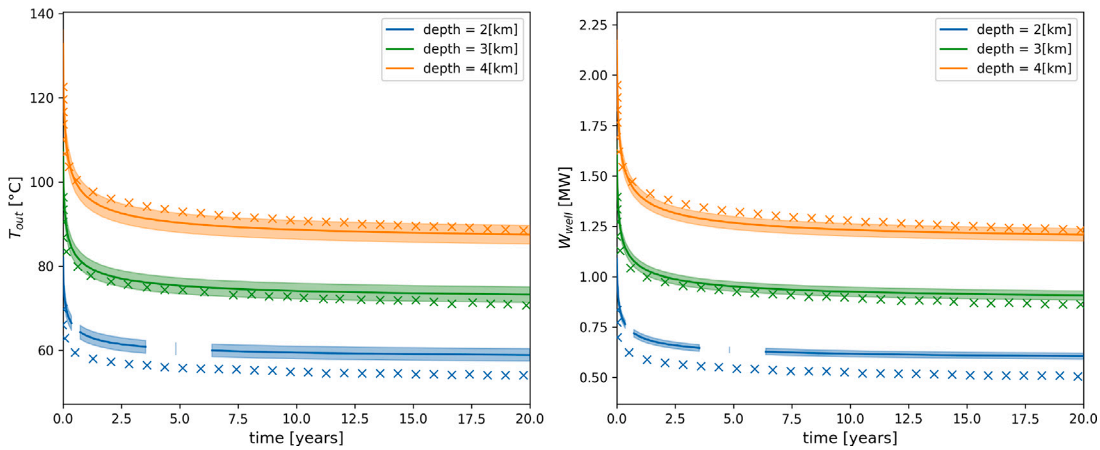

Fig. 4. Validation of the proposed model (plain lines) against results from Wanger et Al. [35] (dots). Shadowed area represent a 2.5% confidence interval.

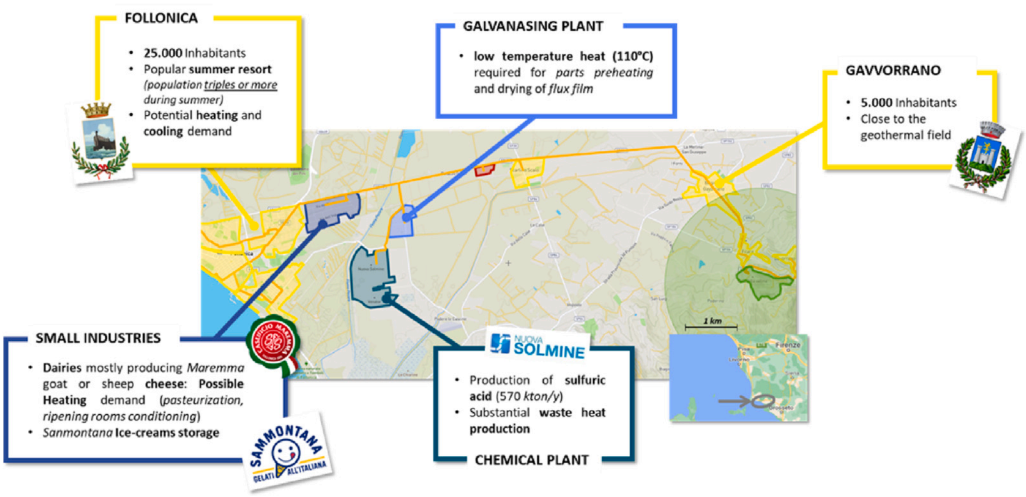

Fig. 5. Area selected for the case study (yellow — municipalities, bluish — industries, green — geothermal resource, orange — DHN) [26].

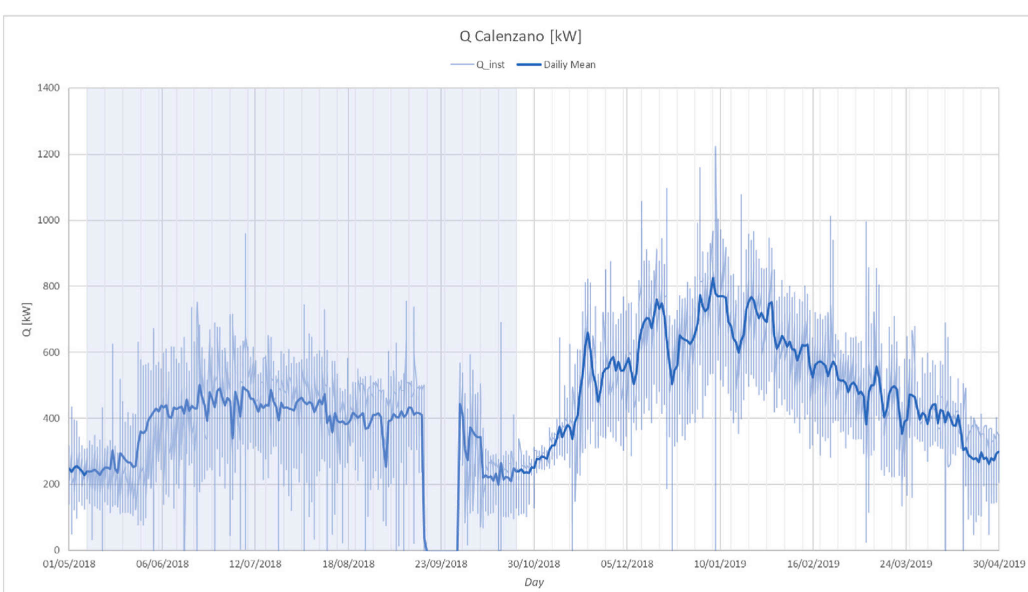

Fig. 6. Calenzano power demand. The shaded area, excluding summer operation for absorption refrigeration, has been considered to estimate the heating demand in this work.

Table 3
Cost correlations used for the economic analysis *(adapted from [36])*.

Comp.	Cost correlation	Notes	Ref.
Well Drilling	$C_{well} = 1.2PPI_{O\&G}(0.105 l_{well}{}^{2} + 1776 l_{well}\phi_{well} + 2.735E5)$	*Result in [$], $PPI_{O\&G}$ inflation adjustment [38], l_{well} length, ϕ_{well} diameter of the well in [m]*	[39]
Pipeline *(CO_2)*	$C_{pipe} = 0.828\phi L$	*Result in [$], pipe diameter in [mm], pipe length in [m]*	[40]
Pipeline *(Water)*	$C_{pipe} = 0.6492\ \phi^{0.9779} L$	*Result in [$], pipe diameter in [mm], pipe length in [m]*	[41]
Heat Exc. *(CO_2)*	$C_{HE} = 49.45 UA_{HE}{}^{0.7544}$	*Result in [$], UA_{HE} in [W/K], it is the product of the HE area and heat transfer coefficient*	[42]
Heat Exc. *(Water)*	$log_{10}(C_{HE}) = 4.6656 - 0.1557 log_{10}(A_{HE}) + 0.1547[log_{10}(A_{HE})]^2$	*Result in [$], A_{HE} is the HE area in [m^2]*	[43]

Table 4
Estimated overall residential heating consumption - Gavorrano area.

Municipality	HDD [°C/day]	Population [-]	Consumption [GWh/y]	Power [MW]
Gavorrano	1748	1000	2.82	0.98
Bagni di Gavorrano	1748	3000	8.47	2.95
Scarlino Scalo	1840	1230	3.61	1.26
Follonica	1527	20,000	50.88	17.75
Total	1577.3	25,230	**65.79**	**22.95**

two refrigeration absorbers in summer to cover the cooling needs of a nearby university campus, so it was excluded from the analysis of this work. $\dot{Q}_{max}$ was calculated by designing the system to cover the requested power up to 2σ. This results in a capacity factor $C_f = 33\%$. Under these conditions, the system is expected to require external power supply for no more than 100 h per year. The estimated heating demand obtained for each municipality are collected in Table 4. Overall consumption is expected to reach approximately 66 GWh/y, with a 2σ peak power demand (on a 15-min resolution) of about 23 MW.

4. Results

4.1. Remarks on system optimization

To optimize the entire system, it is essential to recognize the strong coupling between the performance of the surface system and that of the well. Specifically, the energy conservation equation for the system, expressed in general form in Eq. (15), highlights that, assuming a constant thermal power demand at the user end, an improvement in the thermodynamic performance of the surface system leads to an increased thermal load on the well.

$$\dot{Q}_{DH} = \dot{W}_{net} + \dot{Q}_{well} \tag{15}$$

This is even more clear if we include the Coefficient of Performance (COP) in the equation: to satisfy the user power requirement with a more efficient surface plant, the well power outlet should increase resulting in longer wells and higher costs.

$$\dot{Q}_{well} = \dot{Q}_{DH}\left(1 - \frac{1}{COP}\right) \tag{16}$$

For this reason, the results of this study are presented in two separate sections: the first focuses only on the thermodynamic analysis of the surface system, aimed at evaluating system behavior as a function of key thermodynamic parameters; the latter addresses the economic optimization of the entire system, identifying the optimal solution as the one that minimizes the LCOH value of the whole system.

4.2. Thermodynamic analysis

A detailed thermodynamic analysis was performed for both water and CO_2 proposed configurations.

4.2.1. Water-based layout

To ensure the proper operation of the water-based system, the fluid temperature at the well outlet must exceed the temperature required by the end users. More specifically, a minimum acceptable temperature, referred to as T_{min}, is set at 85 °C, so that the temperature difference between the hot and cold sides of the heat exchangers does not fall below a designated value for each unit. Conversely, a maximum water temperature, referred to as T_{max}, is arbitrary set, for the optimization purposes only, at 200 °C in order to avoid excessively long drilling depths. The thermodynamic analysis of this layout is therefore carried out by introducing a non-dimensional parameter (T_{perc}), used to evaluate the system's performance as a function of the well outlet temperature.

$$T_{perc} = \frac{T_{well,out} - T_{min}}{T_{max} - T_{min}} \tag{17}$$

It is important to highlight that, for given values of depth and geothermal gradient, reaching the desired outlet temperature is only possible for a specific value of $\Delta h_{\%}$ and, consequently, for a corresponding horizontal length. This constraint significantly limits the number of parameters that can be optimized within this layout.

The system's performance as a function of T_{perc} is illustrated in Fig. 7, considering a well depth of 3000 m.

As shown in Fig. 7a, increasing the outlet temperature of the well results in a reduction of both the heat exchanger UA value and the mass flow rate circulating in the network. Both effects are advantageous for the system, as they contribute to decreasing the size of the heat exchangers and the power required for pumping. On the other hand, it is essential to note that, conversely, the value of $\Delta h_{\%}$ must increase to achieve a higher outlet temperature, as shown in Fig. 7b. This effect is particularly detrimental to the system, as it leads to increased drilling costs. These outcomes confirm the theoretical analysis introduced at the start of this section, reinforcing the need to account for economic factors in the comprehensive optimization of the system.

4.2.2. CO_2-based layout

The methodology adopted for the thermodynamic analysis of the CO_2-based layout builds upon that developed for the water-based configuration, with the inclusion of additional parameters to reflect the increased complexity of the system. In particular, the analysis primarily investigates the influence of the supply temperature rather than the well outlet temperature, as these parameters are decoupled through the introduction of a liquid separator. Furthermore, two additional parameters are considered to perform a detailed thermodynamic analysis of the heat pump: the regenerative heat exchanger efficiency (HE_{eff}), and a non-dimensional pressure parameter (p_{perc}), defined as:

$$p_{perc} = \frac{p_3 - p_{min}}{p_{max} - p_{min}} \tag{18}$$

where p_{min} corresponds to the pressure required to reach the minimum necessary temperature at the substation heat exchanger and p_{max} is

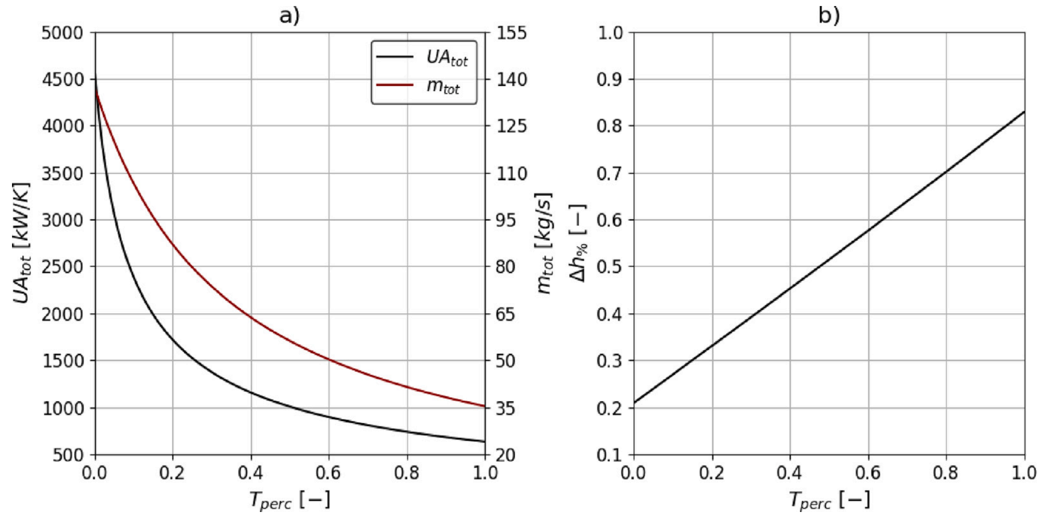

Fig. 7. Water-based layout thermodynamic analysis: effect of T_{perc}.

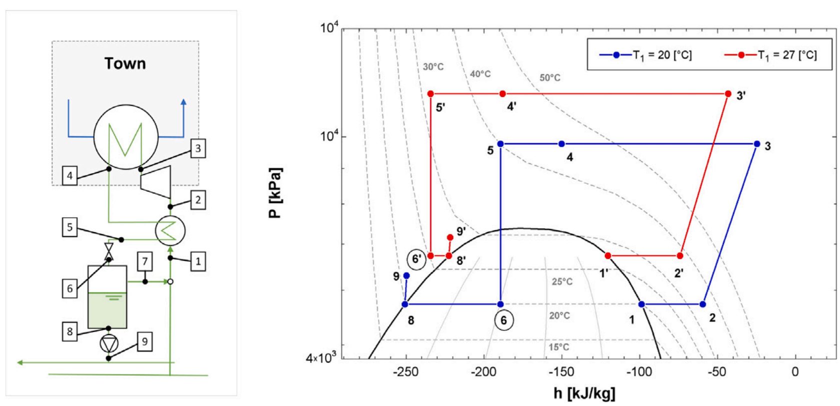

Fig. 8. P-h diagram - Thermodynamic cycle.

fixed at 300 bar. p_3 corresponds to the maximum pressure in the heat pump unit, as illustrated in Fig. 8.

The effect of p_{perc} and HE_{eff} is shown in Fig. 9, focusing on the compression work. As expected, increasing the gas cooler pressure leads to a rise in compression work due to the greater enthalpy difference across the compressor. Conversely, a higher regenerative heat exchanger efficiency results in a reduction of the required compression work. This outcome is attributed to the increased inlet temperature of the working fluid, which allows the compressor to reach the target temperature with a lower discharge pressure p_3.

The other parameter strongly affecting system performance is the saturation temperature of CO_2 in the DH network pipeline (T_{supply}). As shown in Fig. 10, decreasing T_{supply} increases the compressor power demand, which is expected since the final target temperature after compression remains fixed.

At first glance, lowering T_{supply} could be beneficial, as it would reduce the turbine outlet temperature and thus increase the turbine power output. However, Fig. 10 shows the opposite: the energy recovered by the turbine increases with T_{supply}. This effect is explained by the interplay between back-pressure and flow rate. Although a higher T_{supply} increases the turbine back-pressure, thereby reducing the specific turbine work, this loss is more than offset by the higher mass flow rate circulating in the well.

The increase in flow rate occurs because the reduced compression power of the localized heat pumps (as explained in Section 4.1 by Eq. (16)) requires a higher power extraction from the well — thus a higher flow rate.

Summarizing, because of a combination of effects as shown in Fig. 10, increasing T_{supply} always results in a decrease of overall electrical power requirements from the surface equipment (considering that the power delivered to the DH network is fixed to 23MW, the COP of the surface plant in the condition above lies between 4.6 and 7.6).

However, it is important to note that reducing the absorbed work implies an increased demand for thermal energy extracted from the well in order to supply the same heating power to the end users. This requirement can only be met by extending the drilling length, thereby incurring higher capital costs. As previously emphasized, a comprehensive optimization of the system must incorporate economic considerations.

4.3. Economic analysis

Regarding economic analysis, particular emphasis was placed on determining the optimal geometry of the well, which constitutes the primary cost associated with geothermal solutions. The analysis included the required depth and horizontal length as geometric design parameters. The diameter of the well was assumed to be constant at 0.25 m.

4.3.1. Water-based network behavior

In the water-based network, selecting a value of T_{perc} corresponds to fixing the outlet fluid temperature, as can be seen in Fig. 11. For each depth, this choice uniquely determines the horizontal length required to achieve the specified temperature. This means that we can use the

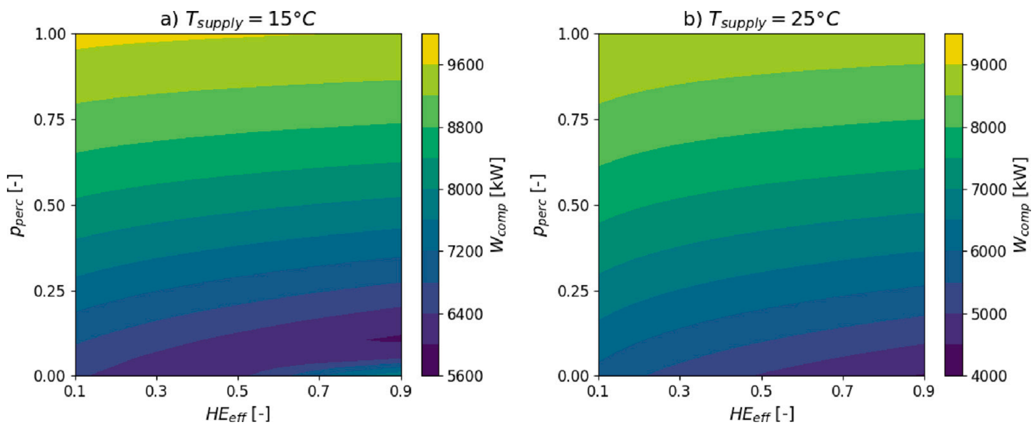

Fig. 9. Effect of p_{perc} and HE_{eff} on the compression work.

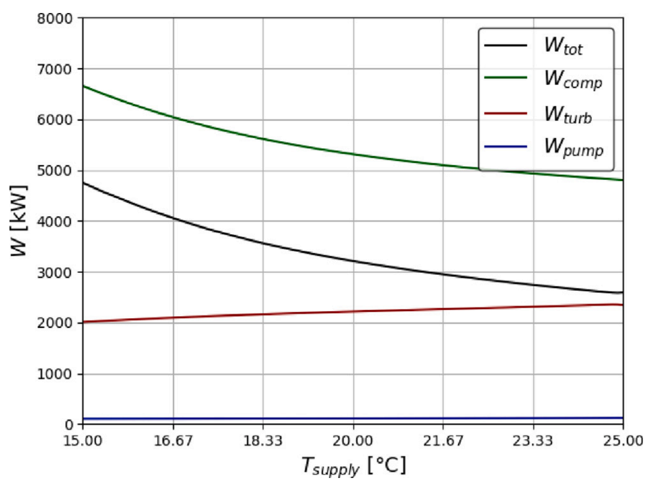

Fig. 10. Electric power values in the network as a function of network supply temperature.

economic optimization based on T_{perc} to identify the optimal horizontal length.

It is interesting to note that, at lower depths, the optimal value of T_{perc} is fixed at 0. This implies that a certain horizontal length is required solely to achieve a sufficiently high surface temperature to supply the district heating network. At greater depths, however, there is more flexibility in selecting the outlet temperature, with both the optimal T_{perc} and the required horizontal length increasing as depth increases.

4.3.2. CO_2 -based network behavior

The CO_2-based network is more flexible, so a more detailed parametric analysis was required to identify the optimal horizontal length for each depth. The results of this analysis are presented in Fig. 12 for a representative depth of 3500 m.

As shown in Fig. 12, the electrical power consumed by the system decreases with the increase in supply temperature, aligning with the findings discussed in the previous subsection. However, a reduction in saturation temperature significantly decreases drilling costs, in part because heat extraction becomes easier thanks to the higher temperature difference between the fluid and the rocks, but mainly because of an actual decrease of the heat to be extracted from the well which is compensated by the power provided by the compressors, resulting in the minimum LCOH (Fig. 12). Furthermore, for the given depth, an optimal value of the horizontal length around 2.5 km minimizes the LCOH, almost independently of supply temperature. Notice in this configuration that the surface plant power requirements lies between 8 and 9 MW resulting in a COP between 2.5 and 2.9.

4.3.3. Remarks on flow rate selection

The optimal length just shown depends on the flow rate circulated in the wells. Increasing the mass flow rate circulating in the well is generally beneficial, as it reduces the number of wells required to meet the heat demand of municipalities. However, this comes at the cost of longer well lengths to maintain the same performance as at lower flow rates, as shown in Fig. 13. The benefit of higher flow rates arises because the well cost correlation (see Table 3) includes a fixed cost component, making fewer, longer wells preferable to more, shorter ones. The reduction in LCOH, however, tends to level off at higher flow rates.

The optimal flow rate ultimately depends on pressure losses in the well, which can render higher flow rates unfeasible (illustrated in Fig. 13, right panel, dashed lines). Since the simplified model does not include pressure loss calculations — which requires a more detailed description of well geometry to be evaluated losing generality — it is not possible to identify an exact optimal flow rate. To address this, flow rates of 5 kg/s for water and 10 kg/s for CO_2 were considered, which are slightly lower than the optimal values reported in the literature [21,35]. As a result, the LCOH values presented hereafter are slightly overestimated.

Summarizing, increasing the flow rate does not significantly affect the LCOH but shifts the optimal solution toward fewer, longer wells. For instance, increasing the flow rate from 10 to 15 kg/s under the conditions shown in Fig. 13 leads to a minor reduction in LCOH from 16.2 to 15.4c€/kWh, while the optimal horizontal length increases from 2.5 km to 3.5 km and the required number of wells decreases from 9 to 6. Thus, while the LCOH estimates presented below are robust, the predicted optimal well length remains sensitive to the selected flow rate per well and should be regarded as an approximate indication.

4.3.4. Overall comparison

The optimal solutions for both configurations are compared in Fig. 14 as a function of depth.

Fig. 14 on the left shows that the optimal horizontal length of the CO_2-based layout is generally shorter than that required for the water-based configuration. This result arises from the lower outlet temperature required in the CO_2-based system, which can be compensated by the surface plant, enabling a more compact and cost-effective geothermal layout. The associated reduction in drilling costs represents a key factor in the overall economic optimization of the system, as illustrated in Fig. 14 on the right. At shallow depths, the water-based configuration requires extremely long horizontal sections to maintain a sufficiently high outlet temperature, resulting in very high LCOH values. By contrast, the CO_2-based system can offset this limitation

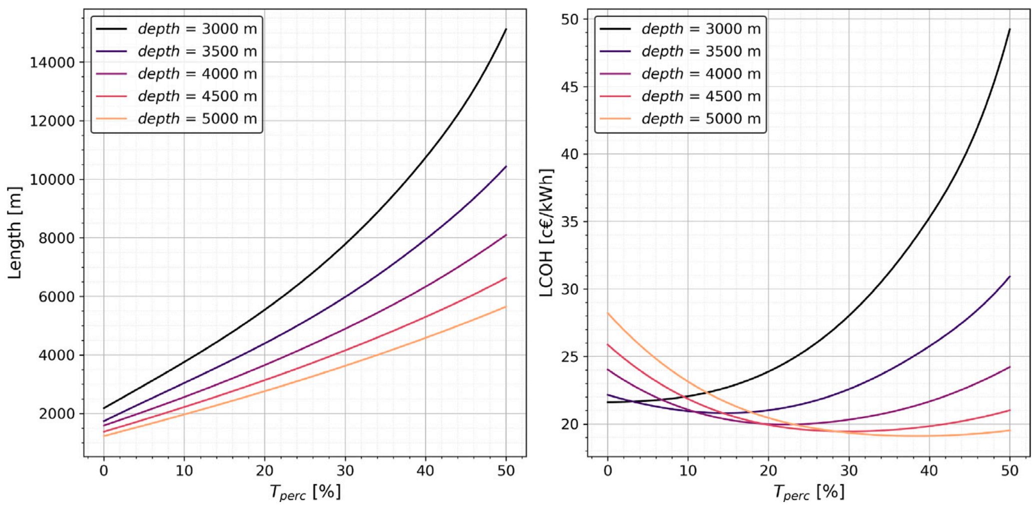

Fig. 11. Analysis of the economic effect of T_{perc} for the water-based solution.

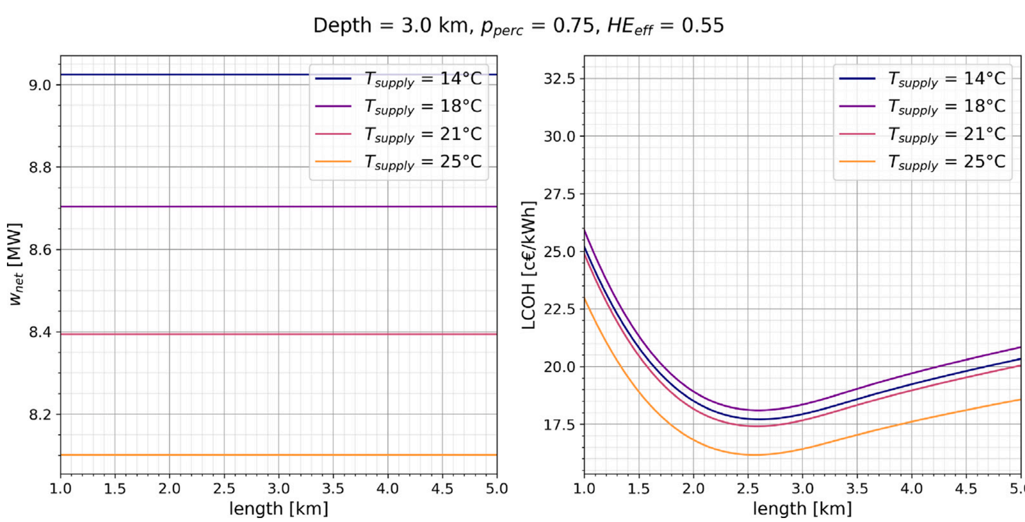

Fig. 12. Analysis of the economic effect of horizontal section length for the CO_2-based solution.

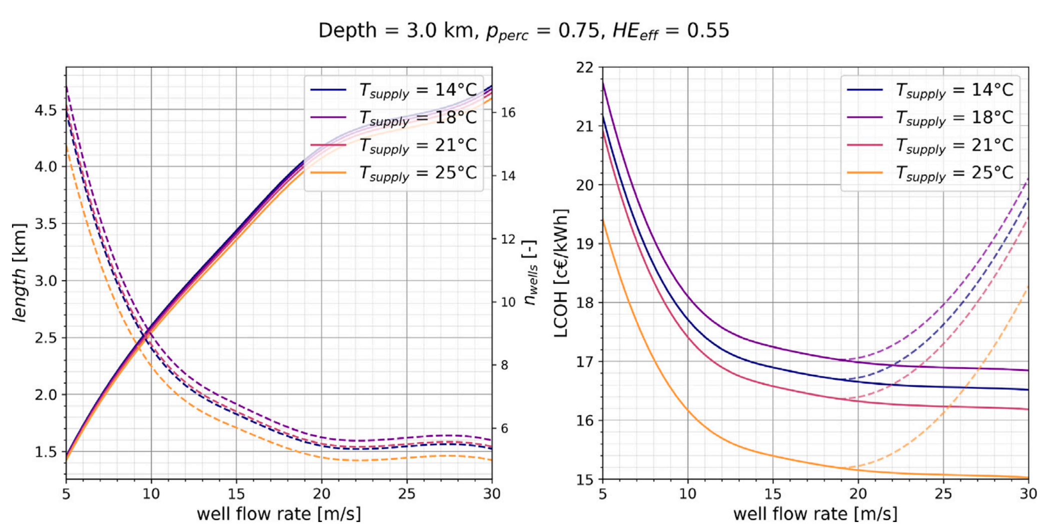

Fig. 13. Effect of flow rate on the economics of the CO_2-based solution. On the left: horizontal section length (plain line) and number of wells to be drilled. On the right: evaluated LCOH for the given flow rate (plain line), the dashed lines represent possible LCOH trends when accounting for pressure losses; they are illustrative and not direct simulation results.

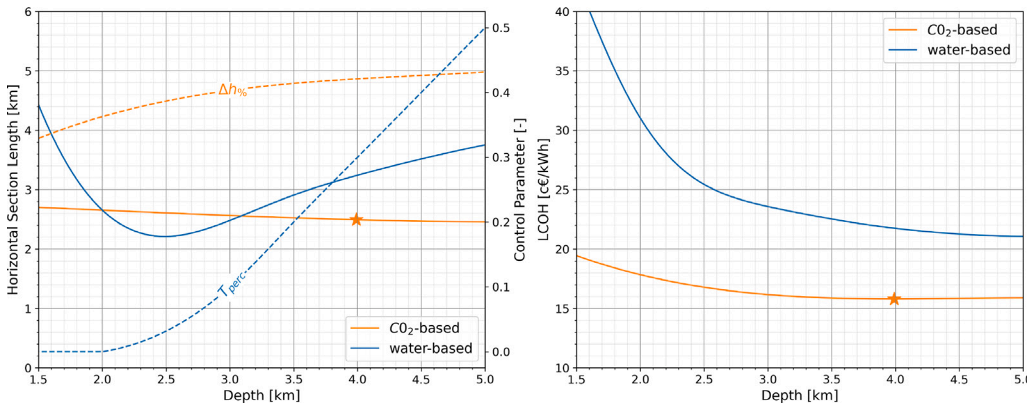

Fig. 14. CO_2-based vs water-based economic analysis comparison.

through higher electricity consumption in the surface plant — the optimal COP from an economic point of view is 3 and is almost independent of depth. In both cases, the most favorable solutions are achieved at greater depths, where rock temperatures are significantly higher. For the CO_2-based network, the optimal LCOH is approximately 0.16 €/kWh, corresponding to a depth of 4 km and a horizontal length of about 2.5 km. In contrast, the water-based network — generally requiring longer horizontal sections — does not reach an optimal LCOH within the considered depth range; at 5 km depth, it achieves an LCOH of 0.21€/kWh with a horizontal section of 3.8 km.

The behavior of the main optimization parameter ($\Delta h_{\%}$ for CO_2 and T_{perc} for water) is also shown in Fig. 14 on the left. For CO_2, the optimal value of $\Delta h_{\%}$ increases slightly with depth, indicating that as geological conditions become more favorable, the economic optimum shifts toward drilling longer wells for obtaining better outlet conditions. In the water-based case, the optimal T_{perc} remains fixed at 0 up to a depth of 2 km, meaning that the well struggles even to reach the minimum required outlet temperature. At greater depths, as rock temperature increases, the optimal T_{perc} begins to rise, allowing for a higher specific heat extraction and a reduction in the number of wells to be drilled.

Finally, Fig. 15 presents a comparison of the LCOH values obtained in this study with those reported in the literature. It has been revealed that they are slightly higher than typical values associated with other heating technologies.

However, some key aspects regarding the conservative criteria used in the study may explain this behavior:

- The design of the geothermal wells was based on the assumption that the system must meet the thermal demand up to 2σ after 20 years of continuous operation. However, this assumption is highly conservative, predicting significant heat transfer degradation due to rock cooling. In practice, the system, which operates intermittently and is expected to meet a generally lower demand, will not lead to such a drastic decrease in rock temperature. Consequently, more compact systems can be developed, decreasing substantially the LCOH of the proposed solutions.
- The potential presence of moving water near the geothermal system, while plausible in the Gavorrano area [47] was not considered in the design of the geothermal wells. Water movement could enhance heat exchange mechanisms, potentially further reducing the cost of both solutions.
- Despite what generally happens with traditional heating systems, the predicted LCOH value is dominated by the initial capital investment. In this sense, once the initial investment is covered, operational costs will be extremely limited and not much affected by the foreseeable change of other primary energy sources, such as natural gas and electrical energy.

These considerations, which will be examined in detail in future works, could substantially lower the cost of geothermal wells and improve the competitiveness of the system compared to other geothermal-based district heating solutions. Finally, it must be noted that closed-loop geothermal systems, even though more expensive, generally have a lower environmental impact on the underground compared to other geothermal systems such as Enhanced Geothermal Systems (EGS). The proposed solutions have a lower risk of induced seismicity and aquifer contamination, making them more socially acceptable for future developers and policymakers.

5. Conclusions

A thermodynamic and economic analysis of an innovative closed-loop geothermal district heating network has been performed. Two different options, based on water and CO_2 as underground and surface heat carrier fluids from a geothermal reservoir, were compared by developing thermodynamic and economic models of both configurations.

Results indicate that the CO_2-based solution provides clear advantages: it reduces drilling depth from 5 to 4 km and lowers the Levelized Cost of Heat (LCOH) from 0.21 to 0.16 €/kWh, thanks to higher operational flexibility and the exploitation of latent heat. In contrast, the water-based network requires deeper and more expensive wells to guarantee supply temperatures. In addition, while is true that the CO_2-based system reach its optimum at 4 km depth, very similar LCOH values are reached even with wells as shallow as 2 km, which are technically easier to drill.

The conservative assumptions adopted in this work suggest that the estimated costs are likely overestimated; future developments, including dynamic well modeling and sensitivity analyses, could further improve the economic competitiveness of both options. Overall, the results highlight the strong potential of CO_2 as an innovative working fluid for geothermal district heating, particularly in enabling the exploitation of shallow and medium-temperature reservoirs while reducing installation costs.

To summarize here are some of the key outcome of this work:

- CO_2-based networks reduce drilling depth and heat cost compared to water-based systems.
- Operational flexibility of CO_2 allows efficient use of shallow and low-temperature geothermal resources.
- Despite the conservative economic estimates, the analyzed technology is comparable with some of the existing alternatives.
- CO_2 shows strong potential as an innovative fluid for sustainable and cost-effective district heating.

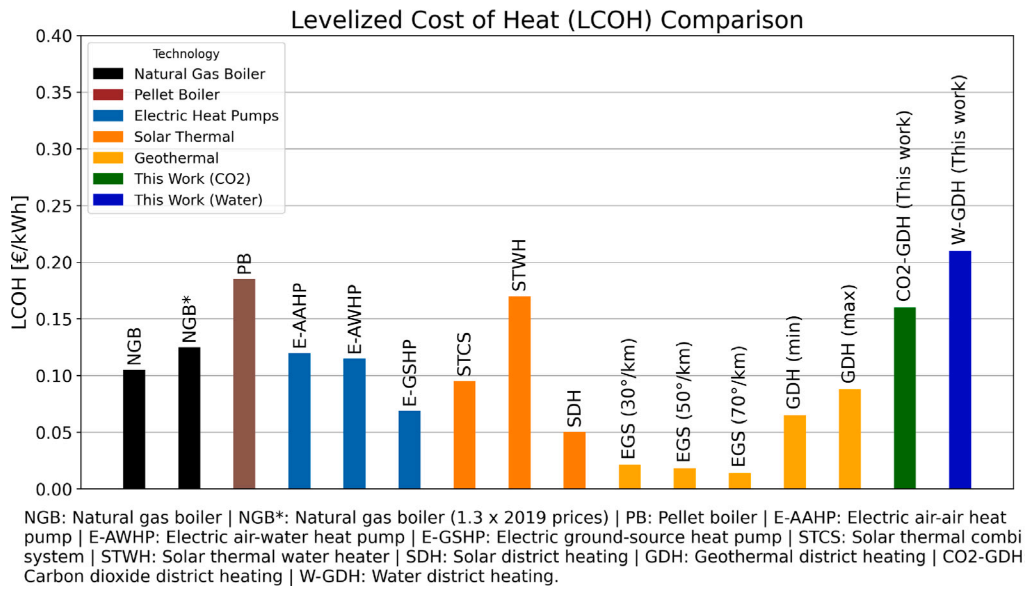

Fig. 15. LCOH of different technologies, the two graph on the extreme right are the proposal for the current work.
Source: Data Sources: [10,13–16,46].

CRediT authorship contribution statement

Daniele Fiaschi: Writing – review & editing, Supervision, Funding acquisition. **Federico Gigliotti:** Writing – review & editing, Writing – original draft, Software, Methodology, Investigation. **Andrés Meana-Fernández:** Writing – review & editing, Writing – original draft, Software, Methodology, Investigation, Formal analysis.

Declaration of competing interest

The authors declare that they have no known competing financial interests or personal relationships that could have appeared to influence the work reported in this paper.

Acknowledgments

The University of Florence, Italy contribution has been financed trough the participation to the HOCLOOP European project *(Horizon Europe Program, Call: HORIZON-CL5-2021-D3-03, Project ID:* 101083558).

Appendix. Rocks heat transfer derivation

Evaluation of R_{rocks}

To determine the horizontal section length required to achieve a given $\Delta h_{\%}$, it was necessary to characterize the heat transfer between the surrounding rocks and the working fluid. A correlation developed by Ungar [32], was used for this purpose:

$$R_{rocks} = \frac{\phi_{well}}{2k_{rocks} f(t_d)} \tag{19}$$

Here, R_{rocks} denotes the conductive thermal resistance between the well and the rocks. $f(t_d)$ is a dimensionless function describing the temporal evolution of this resistance, which increases with time as the surrounding rocks cool. Finally, t_d is the dimensionless time, defined as:

$$t_d = 4\alpha_{rocks} t/\phi_{well}^2 \tag{20}$$

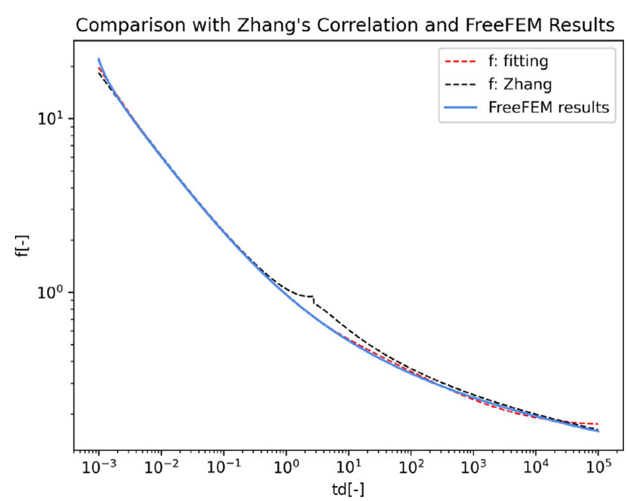

Fig. 16. Comparison of the developed correlation, the FEM analysis results [32] and the $f(t_d)$ employed by [34].

Where α_{rocks} and k_{rocks} are respectively the thermal diffusivity and conductivity of the rock. $f(t_d)$ has been derived from FEM calculations and has the following form:

$$f(t_d) = c_0 + \sum_{i=0}^{n} K_i \left(a_i\, t_d^{b_i} \right) \tag{21}$$

Where K_i are K-Bessel functions of the ith order. The coefficients c_i have been fitted starting from some FEM results [32] and are shown in the Table below for $n = 2$ which is enough to correctly reproduce the behavior of the well for the entirety of its lifespan (see Fig. 16 and Table 5).

Eq. (21) can be also used to evaluate the recovery of the rock heat transfer resistance one the production stops but this requires implementing a convolution approach that will slow down the computation.

Table 5
Parameters for the fitting equation with 3 fitting K Bessel functions.

	$c_0 = 0.7160$	
i	a_i	b_i
0	2.1718	0.5922
1	2.1617	0.5057
2	5.3321	0.3970

Derivation of the formula for heat transfer between well and rocks

Starting from R_{rocks} (as defined in Eq. (19)), the thermal power exchanged between the fluid and the rocks can be determined as:

$$d\dot{q} = \Delta T(h)\frac{\pi\phi_{well}}{R_{rocks}}dx \tag{22}$$

where $\Delta T(h)$ is the temperature difference between undisturbed rocks and the working fluid at a given enthalpy level h. As the fluid is heated up by the surrounding rocks, its temperature and enthalpy increase, and $\Delta T(h)$ is reduced, requiring a higher heat exchange surface for the following pocket of heat. Since $d\dot{q} = \dot{m}\,dh$, it may be written:

$$\frac{dh}{\Delta T(h)} = \frac{\pi\phi_{well}}{R_{rocks}\dot{m}}dx \tag{23}$$

If the convective resistance within the fluid is neglected, as it is generally small compared to conduction resistance across the rocks, R_{rocks} can be considered independent of the fluid condition. Thus, Eq. (23) can be integrated on both sides independently:

$$\Delta h_{max}\int_0^{\Delta h_{\%}} \frac{dh'}{\Delta T(h')} = \int_0^{length} \frac{\pi\phi_{well}}{R_{rocks}\dot{m}}dx = \frac{\pi\phi_{well}}{R_{rocks}\dot{m}}length \tag{24}$$

This relationship allows to determine $length$ once the integral on the left-hand side of Eq. (24) is numerically computed, as shown in Fig. 3:

$$length = \frac{R_{rocks}\dot{Q}_{max}}{\pi\phi_{well}}\int_0^{\Delta h_{\%}} \frac{dh'}{\Delta T(h')} \tag{25}$$

Data availability

Data will be made available on request.

References

[1] IEA, Global Energy Review 2025, Tech. Rep., International Energy Agency, Paris, 2025, URL https://www.iea.org/reports/global-energy-review-2025.

[2] A. Olabi, M. Mahmoud, B. Soudan, T. Wilberforce, M. Ramadan, Geothermal based hybrid energy sytems, towards eco-friendly energy approaches, Renew. Energy 147 (2020) 2003–2012, http://dx.doi.org/10.1016/j.renene.2019.09.140.

[3] IEA, The Future of Geothermal Energy, Tech. Rep., International Energy Agency, Paris, 2024, URL https://www.iea.org/reports/the-future-of-geothermal-energy.

[4] E. Barbier, Geothermal energy technology and current status: an overview, Renew. Sustain. Energy Rev. 6 (1) (2002) 3–65, http://dx.doi.org/10.1016/S1364-0321(02)00002-3, URL https://www.sciencedirect.com/science/article/pii/S1364032102000023.

[5] E. Barbier, Nature and technology of geothermal energy: a review, Renew. Sustain. Energy Rev. 1 (1997) 1–69, http://dx.doi.org/10.1016/S1364-0321(97)00001-4.

[6] S. Werner, International review of district heating and cooling, Energy 137 (2017) 617–631, http://dx.doi.org/10.1016/j.energy.2017.04.045.

[7] C. Breyer, S. Khalili, D. Bogdanov, M. Ram, A.S. Oyewo, A. Aghahosseini, A. Gulagi, A.A. Solomon, D. Keiner, G. Lopez, P.A. Ostergaard, H. Lund, B.V. Mathiesen, M.Z. Jacobson, M. Victoria, S. Teske, T. Pregger, V. Fthenakis, M. Raugei, H. Holttinen, U. Bardi, A. Hoekstra, B.K. Sovacool, On the History and Future of 100% Renewable Energy Systems Research, IEEE Access 10 (2022) 78176–78218, http://dx.doi.org/10.1109/ACCESS.2022.3193402.

[8] M.Z. Jacobson, A.-K. von Krauland, S.J. Coughlin, E. Dukas, A.J.H. Nelson, F.C. Palmer, K.R. Rasmussen, Low-cost solutions to global warming, air pollution, and energy insecurity for 145 countries, Energy Environ. Sci. 15 (8) (2022) 3343–3359, http://dx.doi.org/10.1039/D2EE00722C.

[9] IEA, Levelized cost of heating (LCOH) for consumers, for selected space and water heating technologies and countries, 2021.

[10] J. Huang, J. Fan, S. Furbo, Feasibility study on solar district heating in China, 2019, http://dx.doi.org/10.1016/j.rser.2019.03.014.

[11] G. Manente, A. Lazzaretto, I. Molinari, F. Bronzini, Optimization of the hydraulic performance and integration of a heat storage in the geothermal and waste-to-energy district heating system of ferrara, J. Clean. Prod. 230 (2019) 869–887, http://dx.doi.org/10.1016/j.jclepro.2019.05.146.

[12] J.W. Lund, A.N. Toth, Direct utilization of geothermal energy 2020 worldwide review, Geothermics 90 (2021) 101915, http://dx.doi.org/10.1016/j.geothermics.2020.101915.

[13] P. Olasolo, M.C. Juárez, J. Olasolo, M.P. Morales, D. Valdani, Economic analysis of Enhanced Geothermal Systems (EGS). A review of software packages for estimating and simulating costs, (ISSN: 13594311) 2016, pp. 647–658, http://dx.doi.org/10.1016/j.applthermaleng.2016.05.073.

[14] A. Molar-Cruz, M.F. Keim, C. Schifflechner, M. Loewer, K. Zosseder, M. Drews, C. Wieland, T. Hamacher, Techno-economic optimization of large-scale deep geothermal district heating systems with long-distance heat transport, Energy Convers. Manage. 267 (2022) http://dx.doi.org/10.1016/j.enconman.2022.115906.

[15] A.S. Pratiwi, E. Trutnevyte, Decision paths to reduce costs and increase economic impact of geothermal district heating in Geneva, Switzerland, Appl. Energy 322 (2022) http://dx.doi.org/10.1016/j.apenergy.2022.119431.

[16] M. White, Y. Vasyliv, K. Beckers, M. Martinez, P. Balestra, C. Parisi, C. Augustine, G. Bran-Anleu, R. Horne, L. Pauley, G. Bettin, T. Marshall, A. Bernat, Numerical investigation of closed-loop geothermal systems in deep geothermal reservoirs, Geothermics 116 (2024) http://dx.doi.org/10.1016/j.geothermics.2023.102852.

[17] D. Brown, A hot dry rock geothermal energy concept utilizing supercritical CO2 instead of water, Twenty-Fifth Work. Geotherm. Reserv. Eng. (2000).

[18] K. Pruess, Enhanced geothermal systems (EGS) using CO2 as working fluid - A novel approach for generating renewable energy with simultaneous sequestration of carbon, Geothermics 35 (4) (2006) 351–367, http://dx.doi.org/10.1016/j.geothermics.2006.08.002.

[19] M. Tagliaferri, P. Gładysz, P. Ungar, M. Strojny, L. Talluri, D. Fiaschi, G. Manfrida, T. Andresen, A. Sowiżdżał, Techno-Economic Assessment of the Supercritical Carbon Dioxide Enhanced Geothermal Systems, Sustainability 14 (24) (2022) 16580, http://dx.doi.org/10.3390/su142416580.

[20] A.D. Atrens, H. Gurgenci, V. Rudolph, Electricity generation using a carbon-dioxide thermosiphon, Geothermics 39 (2) (2010) 161–169, http://dx.doi.org/10.1016/j.geothermics.2010.03.001.

[21] A.E. Malek, B.M. Adams, E. Rossi, H.O. Schiegg, M.O. Saar, Techno-economic analysis of Advanced Geothermal Systems (AGS), Renew. Energy 186 (2022) 927–943, http://dx.doi.org/10.1016/j.renene.2022.01.012.

[22] P. Ungar, D. Fiaschi, G. Manfrida, L. Talluri, Thermodynamic Assessment of Geothermal High-Temperature Heat Pumps for Industrial Steam Production, Available At SSRN (2023) http://dx.doi.org/10.2139/ssrn.4350038.

[23] C. Weber, D. Favrat, Conventional and advanced CO2 based district energy systems, Energy 35 (12) (2010) 5070–5081, http://dx.doi.org/10.1016/j.energy.2010.08.008.

[24] P. Ungar, L. Milli, G. Manfrida, D. Fiaschi, L. Talluri, Re-designing district heating networks through innovative CO2 solutions, J. Phys.: Conf. Ser. 2385 (1) (2022) 012125, http://dx.doi.org/10.1088/1742-6596/2385/1/012125.

[25] D. Romanov, B. Leiss, Geothermal energy at different depths for district heating and cooling of existing and future building stock, 2022, http://dx.doi.org/10.1016/j.rser.2022.112727.

[26] B. Laenen, V. Harcouët-Menou, M. Singh, C. Souque, D. Liotta, D. Fiaschi, Pilot Sites Data and Integration Analysis D4.1, Tech. Rep., 2023.

[27] European Project, A circular by design environmentally friendly geothermal energy solution based on a horizontal closed loop - HOCLOOP, 2022.

[28] A. Brogi, A. Caggianelli, D. Liotta, M. Zucchi, A. Spina, E. Capezzuoli, A. Casini, E. Buracchi, The gavorrano monzogranite (Northern apennines): An updated review of host rock protoliths, thermal metamorphism and tectonic setting, Geosci. (Switzerland) 11 (3) (2021) 1–31, http://dx.doi.org/10.3390/geosciences11030124.

[29] D.M. 26.6.2009, n. 158, "Linee guida nazionali per la certificazione energetica degli edifici", (Italian).

[30] H. Li, S. Svendsen, Energy and exergy analysis of low temperature district heating network, Energy 45 (1) (2012) 237–246, http://dx.doi.org/10.1016/j.energy.2012.03.056.

[31] S.W. Churchill, Friction-factor equatin spans over all fluid-flow regimes, Chem. Eng. 84 (1977) 91–92.

[32] P. Ungar, Use of CO2 as Working Fluid in Geothermal Systems (Ph.D. thesis), University of Florence, Florence, 2023.

[33] R. DiPippo, Geothermal Power Plants: Principles, Applications, Case Studies and Environmental Impact, Butterworth-Heinemann, 2012.

[34] Y. Zhang, L. Pan, K. Pruess, S. Finsterle, A time-convolution approach for modeling heat exchange between a wellbore and surrounding formation, Geothermics 40 (4) (2011) 261–266, http://dx.doi.org/10.1016/j.geothermics.2011.08.003.

[35] M. Wangen, V. Leontidis, E. Hernandez Acevedo, V. Harcouët-Menou, P. Ungar, Simulation of closed-loop geothermal systems, (ISSN: 2214-4609) 2024, http://dx.doi.org/10.3997/2214-4609.202410516.

[36] P. Ungar, C. Schifflechner, C. Wieland, G. Manfrida, H. Spliethoff, Thermo-Economic Comparison of CO2 and Water as a Heat Carrier for Long-Distance Heat Transport from Geothermal Sources, in: 36th International Conference on Efficiency, Cost, Optimization, Simulation and Environmental Impact of Energy Systems, (ECOS 2023), ECOS 2023, Las Palmas De Gran Canaria, Spain, 2023, pp. 2593–2602, http://dx.doi.org/10.52202/069564-0233.

[37] Gestore dei Servizi Energetici (GSE), MGP - esiti - PUN INDEX GME, 2024, https://gme.mercatoelettrico.org/it-it/Home/Esiti/Elettricita/MGP/Esiti/PUN. (Accessed April 2025).

[38] U.S. Bureau of Labor Statistics, Producer Price Index by Industry: Oil and Gas Extraction. URL https://fred.stlouisfed.org/series/PCU21112111.

[39] B.M. Adams, J. Ogland-Hand, J. Bielicki, P. Schädle, M. Saar, Estimating the Geothermal Electricity Generation Potential of Sedimentary Basins Using genGEO (the generalizable GEOthermal techno-economic simulator), 2021, ChemRxiv Preprint.

[40] G. Heddle, H. Herzog, M. Klett, The economics of CO2 storage, Mass. Inst. Technol. Lab. Energy Environ. (2003).

[41] K.C. Kavvadias, S. Quoilin, Exploiting waste heat potential by long distance heat transmission: Design considerations and techno-economic assessment, Appl. Energy 216 (2018) 452–465, http://dx.doi.org/10.1016/j.apenergy.2018.02.080.

[42] N.T. Weiland, B.W. Lance, S.R. Pidaparti, sCO2 Power Cycle Component Cost Correlations From DOE Data Spanning Multiple Scales and Applications, in: ASME Turbo Expo 2019: Turbomachinery Technical Conference and Exposition, American Society of Mechanical Engineers, Phoenix, Arizona, USA, 2019, http://dx.doi.org/10.1115/GT2019-90493.

[43] R. Turton, R.C. Bailie, W.B. Whiting, J.A. Shaeiwitz, D. Bhattacharyya, Analysis, Synthesis, and Design of Chemical Processes, vol. 40, (6) 2001, p. 9823, http://dx.doi.org/10.1002/1521-3773(20010316)40:6<9823::AID-ANIE9823>3.3.CO;2-C, URL http://ptgmedia.pearsoncmg.com/images/9780132618120/samplepages/0132618125.pdf.

[44] C.A. Garzonio, A. Affuso, Hydrogeological problems for the rehabilitation and re-utilisation of the water resources of the mining area of gavorrano (Italy), Environ. Geol. 46 (2004) 286–294.

[45] P. Baldi, S. Bellani, A. Ceccarelli, A. Fiordelisi, P. Squarci, L. Taffi, Geothermal anomalies and structural features of southern tuscany, in: World Geothermal Congress Proceedings Florence, 1995, pp. 1287–1291.

[46] International Energy Agency (IEA), World energy outlook 2022, 2022, https://www.iea.org/reports/world-energy-outlook-2022. (Accessed May 2025).

[47] A. Minissale, Origin, transport and discharge of CO2 in central Italy, Earth-Sci. Rev. 66 (1–2) (2004) 89–141, http://dx.doi.org/10.1016/j.earscirev.2003.09.001.